Generation of cylindrical vector vortex beams with high purity by using cascaded all-dielectric metasurfaces

XIAODONG ZHANG[1,2,3,*], XINPENG WU[1], JILI ZHANG[1], YU ZHAO[1], NINGTAO MA[1], QIYUAN MU[4]
[1]*School of Physics and Electronic Engineering, Zhengzhou University of Light Industry, Zhengzhou 450002, China*
[2]*Henan Key Laboratory of Magnetoelectronic Information Functional Materials, Zhengzhou University of Light Industy, Zhengzhou 450002, China*
[3]*Zhengzhou Key Laboratory of Information Optics and Photoelectric Technology, Zhengzhou University of Light Industry, Zhengzhou 450002, China*
[4]*Xi'an Institute of Optics and Precision Mechanics, Chinese Academy of Sciences, Xi'an 710119, China*

In this paper, we propose an efficient approach to generate cylindrical vector vortex beams by cascading the three all-dielectric metasurfaces. The cascaded metasurfaces are composed of 21×21 array units, operate at 1550 nm and are capable of generating the cylindrical vector vortex beams with topological charges of ±1 and polarization orders of ±1 under the incidence of circularly polarized light. Mode purity of the cylindrical vector vortex beam is 81.71% calculated by numerical simulation. Our design has characteristics of high purity, compact and easy-fabrication and may be a potential candidate in integrated optical system in future.

(Received April 30, 2022; accepted February 14, 2023)

Keywords: Cascaded metasurfaces, Vortex beam, Vector beam

1. Introduction

Vortex beam[1] characterized by spiral phase wavefront, doughnut-like intensity distribution has attracted a great deal of interests in many field, such as optical manipulation, optical communication, super-resolution and quantum information *etc*.[2-4] Cylindrical vector beam has characteristics of symmetrical polarization distribution on the cross section along the propagation axis[5]. For example, the radially polarized beam can be focused more sharply and give rise to a centered longitudinal field while the azimuthally polarized beam can achieve a significantly smaller size spot than the radially polarized beam in high NA condition. So the unique polarization state makes them have important applications in optical manipulation, high-resolution imaging and optical information processing *etc*.[6, 7] Cylindrical vector vortex (CVV) beam characterized by inhomogeneous polarization distribution and helical wavefront has been widely investigated as a new promising resource due to extra degree of freedom of light manipulation[8-10]. The metasurfaces can be used for controlling the amplitude, polarization and phase of beam in sub-wavelength resolution and have characteristics of allowing abrupt changes of phase, eliminating the higher order diffraction and facilitating strong light-matter interaction on a sub-wavelength scale *etc*.[11-13] while traditional optical elements (such as lens, waveplate *etc*.) have not. The metasurfaces have been widely investigated in many exotic research areas, including abnormal refraction, photonic spin hall effect, super lens and holography *etc*.[14-16] Meanwhile, The advanced nano-fabrication technology enable metasurfaces very promising available for integrated photonic devices[17].

Compared to the characteristics of broadband, indispersion of plasmonic metasurfaces[18-24], all-dielectric metasurfaces have advantages of low absorption loss and high transmission efficiency in the near-infrared band, and soon these advantages have made all-dielectric metasurfaces become a hot spot[25-28]. Some researchers can generate CVV beams by cascading some metasurfaces and traditional optical elements (such as waveplate, spatial light modulator and q-plate *etc*.)[29-31]. However, the equipment composed of the metasurfaces and bulk optical elements undoubtedly brings more difficulty in applying for the integrated optical system. Compared with the reflective type metasurfaces of generating CVV beams[32], the transmission type of our design has a wider application

space.

In this paper, we propose a scheme to generate CVV beams with fixed topological charges and polarization orders based on the three cascaded all-dielectric metasurfaces. The three metasurfaces are all composed of silicon nanopillars and SiO_2 rectangle as the emitter and substrates respectively. The nanopillars in the first and third metasurfaces are distributed with 21×21 array based on the geometric phase[33], and the nanopillars in the second metasurface have the same array distribution but are all rotated by 45° to the x axis. The designed cascaded metasurfaces can be employed to transfer the circularly polarized light to the azimuthally polarized beam or the radially polarized beam with topological charge value of ±1. The transmittance of the cascaded metasurfaces is 88.54%, and the mode purity of the CVV beam reaches 81.71% The designed metasurfaces work at 1550 nm that can be used as a scheme for generating CVV beam in the integrated photonic devices.

2. Theoretical analysis

For all-dielectric metasurfaces, the unit composed of high refractive index materials such as silicon, germanium, tellurium, etc. can support electric and magnetic dipole responses based on Mie resonances[34]. The designed metasurface unit is depicted in Fig.1. The unit is composed of two parts, one is the elliptical Si nanopillar, the other is SiO_2 substrate. The designed nanopillar works as a Fabry-Perot resonator, and the effective refraction index of the waveguide depends on the shape of cross section of the nanopillar[35]. The optimized geometrical parameters of the metasurface unit 1 are set: major radius of r_1=200 nm, minor radius of r_2=100 nm, nanopillar thickness of h_1=1.8 μm, substrate thickness of h_2=1.0 μm and unit constant of d_1=800 nm[36]. The numerical simulations were performed based on the finite difference time domain method. The model with the optimized parameters was built and the incident light ranged from 1.5~1.6 μm illuminated the unit vertically. Periodic boundary conditions were employed along the x and y directions and perfectly matched layer boundary conditions along the z direction. When the linearly polarized (LP) light with polarization direction parallel to r_1 or r_2 respectively was vertically incident on the metasurface unit along the z axis direction, the normalized amplitude and phase shift of the transmitted light are depicted in Fig. 2 (a). Here, t_{ij} represents the tranmittance and its subscripts denote the component i of the transmitted light under the component j of the incident light, and $\Delta\phi$ denote the phase shift between the orthogonal components of the transmitted light. It can be seen that t_{r1r1} and t_{r2r2} both keep high values as close as 1 and $\Delta\phi$ gets to π approximately ($\Delta\phi$ =π at 1550 nm) in the whole band. Thus the designed metasurface unit can be used as half-wave plate at 1550 nm.

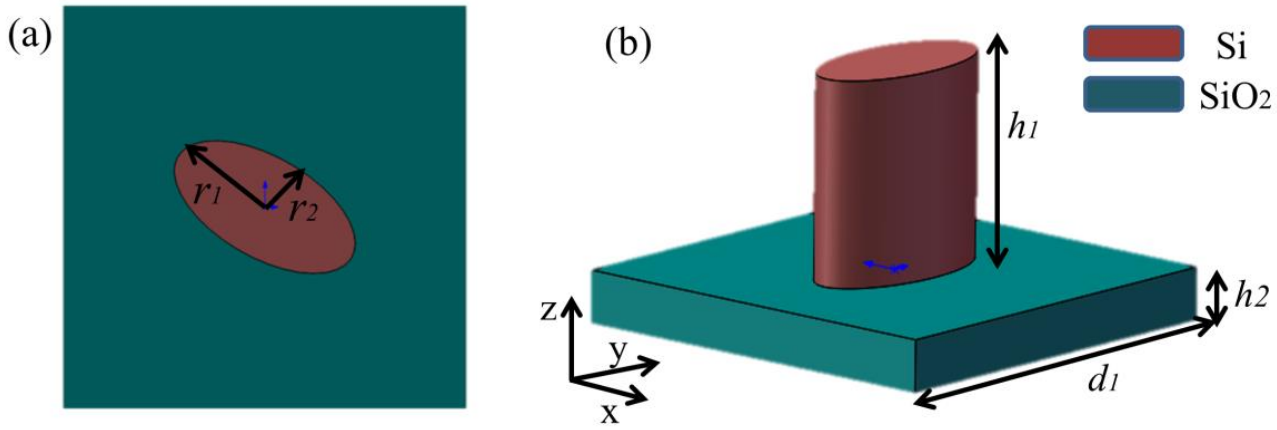

Fig. 1. Schematic of the all-dielectric metasurface unit. (a) Top view of the metasurface unit. (b) 3D view of the metasurface unit (color online)

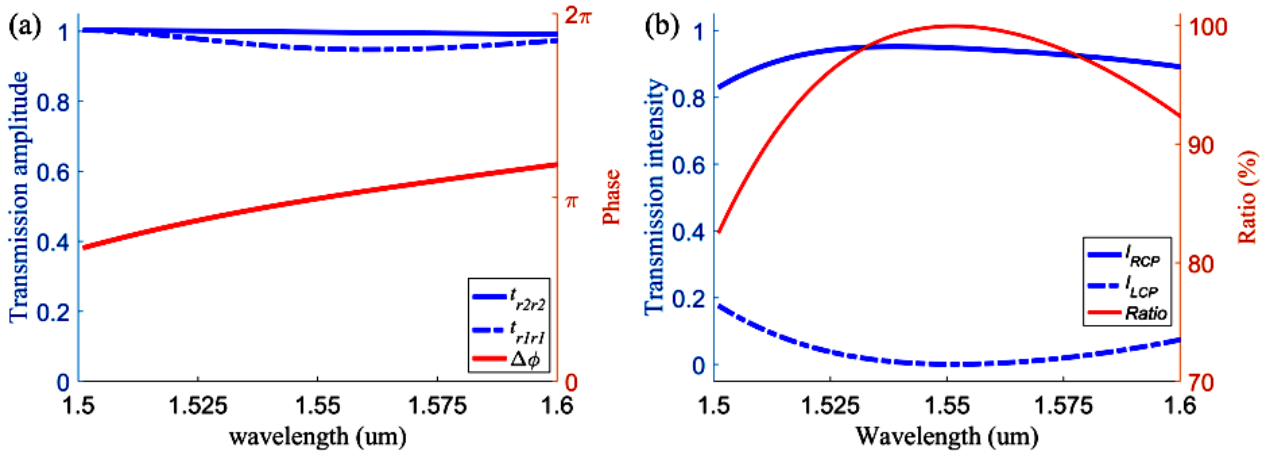

Fig. 2. (a) The normalized amplitude and phase shift of the transmitted light under the LP incident light. (b) The normalized intensity and Ratio of the transmitted light under the LCP incident light (color online)

Generally, Jones matrix acts as a tool for theoretical calculation to represent the function of the optical devices, so the Jones matrix of the metasurface unit can be expressed as $T_{hw}=\begin{bmatrix}1 & 0\\ 0 & e^{\pi i}\end{bmatrix}$, and left circularly polarized (LCP) light and right circularly polarized (RCP) light are denoted as $\begin{bmatrix}1\\ i\end{bmatrix}$ and $\begin{bmatrix}1\\ -i\end{bmatrix}$ respectively. Consequently, under the incidence of the circularly polarized light on the metasurface unit, the Jones expression of the transmitted light is written by:

$$E_{out}^{LCP}=T_{hw}E_{LCP}=\begin{bmatrix}1 & 0\\ 0 & e^{\pi i}\end{bmatrix}\begin{bmatrix}1\\ i\end{bmatrix}=\begin{bmatrix}1\\ -i\end{bmatrix}$$
$$E_{out}^{RCP}=T_{hw}E_{RCP}=\begin{bmatrix}1 & 0\\ 0 & e^{\pi i}\end{bmatrix}\begin{bmatrix}1\\ -i\end{bmatrix}=\begin{bmatrix}1\\ i\end{bmatrix}. \quad (1)$$

We used LCP light as the incident light for validating the performance of the designed metasurface unit and set the wavelength from 1.5 μm to 1.6 μm, the normalized intensity and intensity ratio of the transmitted light are shown in Fig. 2(b). Here, *I*i denotes the transmitted intensity of i component and Ratio is defined as the ratio of the transmitted cross-component intensity to the transmitted intensity. It is obvious that I_{RCP} is greater than 0.9 and I_{LCP} is approximately equal to 0, and Ratio is above 95% at 1550 nm. As a result, the designed metasurface unit can work as half-wave plate with high performance at 1550 nm.

Next, the metasurface unit 2 composed of the elliptic Si nanopillar and the rectangle SiO_2 substrate was designed. The thickness and constant parameters (*h3*, *h4*, d_2) of the unit 2 are the same as those of the metasurface unit 1 except for minor radius of r_3=90 nm and major radius of r_4=179 nm, as shown in Fig. 3(a). The simulation was also employed based on the same incident and boundary conditions. It should be noted that t_{r3r3} and t_{r4r4} both keep high values as close as 1 while $\Delta\varphi$ gets to π/2 approximately ($\Delta\phi$ =π/2 at 1550 nm) in the whole band from Fig. 3(b). So the designed metasurface unit 2 can be used as quarter-wave plate at 1550 nm.

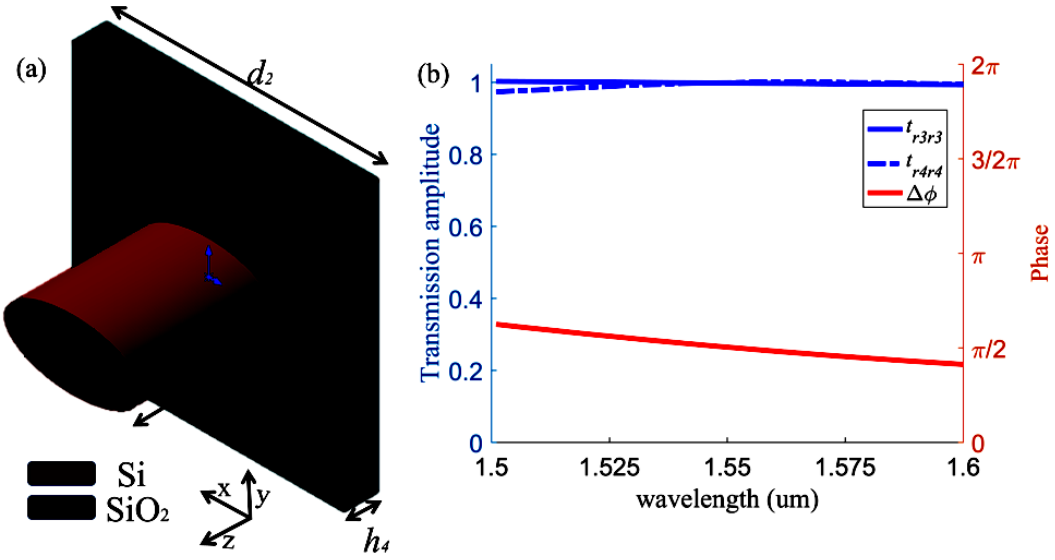

Fig. 3. (a) 3D views of the metasurface unit 2: r_3=90 nm, r_4=179 nm, h_3=1.8 μm, h_4=1 μm, d_2=800 nm. (b)The normalized amplitude and the phase shift of the transmitted light as function of the incident wavelength.

Similarly, the Jones matrix of the metasurface unit 2 can be expressed as $T_{qw}=\begin{bmatrix}1 & 0\\ 0 & e^{\frac{\pi}{2}i}\end{bmatrix}$, and under the incidence of circularly polarized light, the Jones expression of the transmitted light is written by:

$$E_{out}^{LCP}=T_{qw}E_{LCP}=\begin{bmatrix}1 & 0\\ 0 & e^{\frac{\pi}{2}i}\end{bmatrix}\begin{bmatrix}1\\ i\end{bmatrix}=\begin{bmatrix}1\\ -1\end{bmatrix}$$
$$E_{out}^{RCP}=T_{qw}E_{RCP}=\begin{bmatrix}1 & 0\\ 0 & e^{\frac{\pi}{2}i}\end{bmatrix}\begin{bmatrix}1\\ -i\end{bmatrix}=\begin{bmatrix}1\\ 1\end{bmatrix}. \quad (2)$$

We equally used LCP light as the incident light for validating the performance of the designed metasurface unit 2, the normalized intensity and intensity ratio of the transmitted light are depicted in Fig. 4 (a). It is obvious that $I_{135°}$ is greater than 0.95 and $I_{45°}$ is approximately equal to 0, and Ratio is almost 100% at 1550 nm. Meanwhile, the phase shift between the transmitted components along the 135° and 45° directions reaches zero degree at 1550 nm, as shown in Fig. 4 (b). Therefore the designed metasurface unit 2 can work as quarter-wave plate with high performance at 1550 nm.

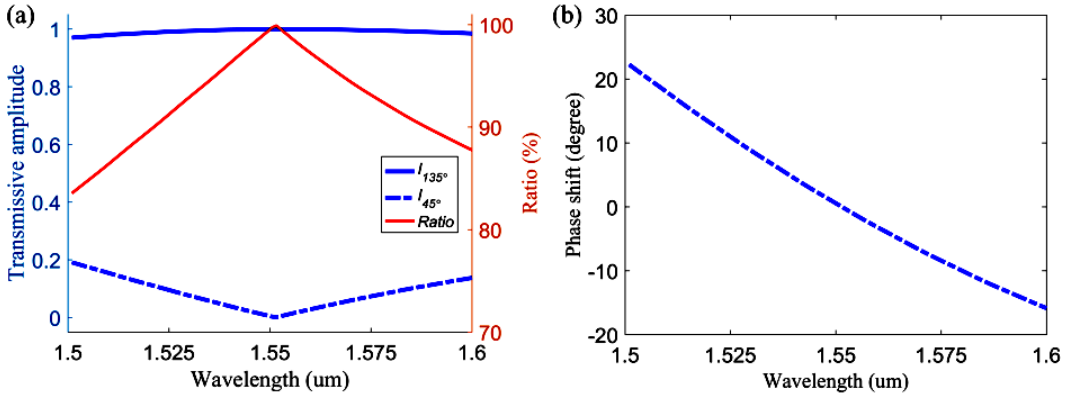

Fig. 4. (a) The normalized intensity and Ratio of the transmitted light under the LCP incident light. (b) The phase shift between the transmitted components along the 135° and 45° directions as function of the incident wavelength (color online)

3. Results and discussions

Firstly, we used the metasurface unit 1 as cell unit and arranged it into 21×21 arrays, then the designed all-dielectric metasurfaces 1 have a size of 17×17 μm, as shown in Fig. 5(a). And, the rotation angle (α) and the azimuthal angle (φ) of every nanopillar satisfies the relation of $\alpha=q\times\varphi+\alpha_0$, q is a constant specifying the topological charge of the vortex beam and α_0 is a constant angle specifying the initial rotation angle for $\varphi=0$, here $q=0.5$, $\alpha_0=90°$. Thus, the Jones matrix of the new metasurfaces 1 can be expressed as:

$$T_{hw}^{'}=\mathrm{M}^{-1}(\alpha_r)T_{hw}M(\alpha_r)=\begin{bmatrix}\cos\alpha_r & -\sin\alpha_r\\ \sin\alpha_r & \cos\alpha_r\end{bmatrix}\begin{bmatrix}1 & 0\\ 0 & e^{\pi i}\end{bmatrix}\times\begin{bmatrix}\cos\alpha_r & \sin\alpha_r\\ -\sin\alpha_r & \cos\alpha_r\end{bmatrix}=\begin{bmatrix}\cos 2\alpha_r & \sin 2\alpha_r\\ \sin 2\alpha_r & -\cos 2\alpha_r\end{bmatrix}=\begin{bmatrix}\cos\varphi & \sin\varphi\\ \sin\varphi & -\cos\varphi\end{bmatrix}, \tag{3}$$

where, $M(\alpha_r)=\begin{bmatrix}\cos\alpha_r & \sin\alpha_r\\ -\sin\alpha_r & \cos\alpha_r\end{bmatrix}$ is unit rotation matrix. When the circularly polarized (CP) light is vertically incident on the metasurfaces 1, neglecting the constant phase, the Jones expression of the transmitted light can be expressed as:

$$T_{out}^{L}=T_{hw}^{'}E_{LCP}=\begin{bmatrix}\cos\varphi & \sin\varphi\\ \sin\varphi & -\cos\varphi\end{bmatrix}\begin{bmatrix}1\\ i\end{bmatrix}=e^{i\varphi}\begin{bmatrix}1\\ -i\end{bmatrix}$$
$$T_{out}^{R}=T_{hw}^{'}E_{RCP}=\begin{bmatrix}\cos\varphi & \sin\varphi\\ \sin\varphi & -\cos\varphi\end{bmatrix}\begin{bmatrix}1\\ -i\end{bmatrix}=e^{-i\varphi}\begin{bmatrix}1\\ i\end{bmatrix}. \tag{4}$$

We can know that the designed metasurfaces 1 can convert the CP light into the cross-polarized with an additional phase ($\pm\varphi$) on the basis of Eq. (4). This additional phase results from space-variant polarization manipulation and is called the geometrical phase[37, 38]. It introduces the spiral wave front distribution which is a direct indication of optical vortex presence and the sign of the topological charge depends on the polarization chirality of the incident CP light.

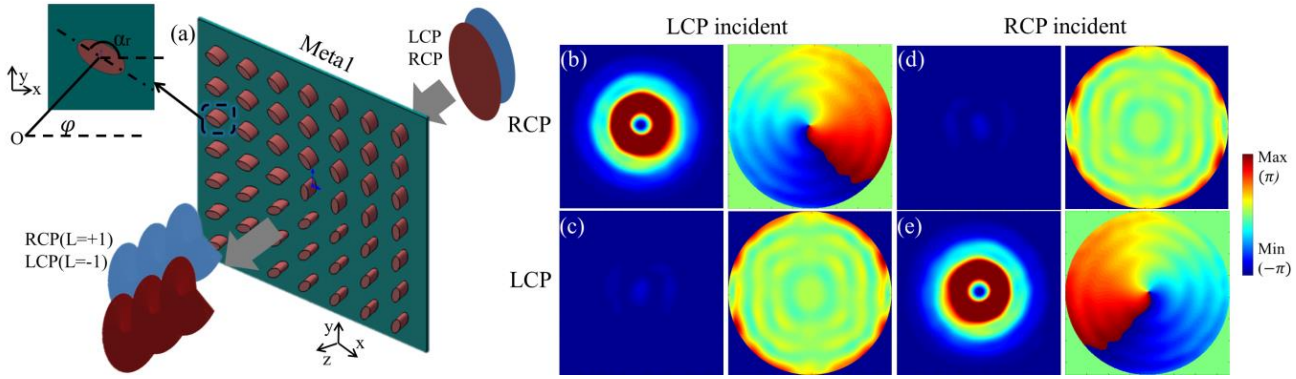

Fig. 5. (a) Schematic of the designed all-dielectric metasurface 1, Inset in (a) shows the relation of the rotation angle (α) and the azimuth angle (φ) of nanopillar. The intensity profile and phase pattern of (b) the RCP component and (c) the LCP component under the LCP incident light. The intensity profile and phase pattern of (d) the RCP component and (e) the LCP component under the RCP incident light

(color online)

We used the CP light at 1550 nm as incident light for validating the performance of the metasurfaces 1, the normalized intensity distribution and phase pattern of the transmitted light are shown in Fig. 5(b)~(e). Obviously for the LCP incident light, the RCP component of the transmitted light has characteristics of the helical phase

pattern and the concentric ring in intensity profile just like 'donut' *etc*. as shown in Fig. 5(b). Transmittance (T) =94.05% and $\frac{I_{RCP}}{I_{out}} = 98.42\%$ was obtained by the numerical calculation. The phase interval from –π to +π and the single petal indicate that the RCP component become the vortex beam with topological charge of +1. Unlike, the LCP component has no characteristics of vortex beam as shown in Fig. 5(c). In contrast, for the RCP incident light, the LCP component has become the vortex beam with topological charge of -1 while the RCP component not. The simulated results prove that the designed metasurfaces 1 is capable of generating vortex beam with charges of ± 1 with high efficiency, the transmitted light is circularly polarized state and the sign of the topological charge is dependent on the handedness of incident CP light, which coincide with the Eq. (4).

Afterwards, we used the metasurface unit 2 as cell unit and arranged it into 21×21 arrays, the designed all-dielectric metasurfaces 2 have a size of 17×17 μm too, as shown in Fig. 6(a). The rotation angle (α) of every nanopillar is set to 45°. So the Jones matrix of the new metasurfaces 2 is written by:

$$T_{qw}^{'}=\mathrm{M}^{-1}(45°)T_{qw}M(45°)=\begin{bmatrix}\cos 45° & -\sin 45°\\ \sin 45° & \cos 45°\end{bmatrix}\begin{bmatrix}1 & 0\\ 0 & e^{\frac{\pi}{2}i}\end{bmatrix}\times\begin{bmatrix}\cos 45° & \sin 45°\\ -\sin 45° & \cos 45°\end{bmatrix}=\begin{bmatrix}2+2i & 2-2i\\ 2-2i & 2+2i\end{bmatrix}. \quad (5)$$

Then, we cascaded the metasurfaces 1 and the metasurfaces 2, and set the distant between the two metasufaces to L (L=5 μm), as shown in Fig. 6(a). When the CP light pass through the two metasurfaces in sequence, neglecting the constant phase, the Jones expression of the transmitted light can be expressed as:

$$\begin{aligned}T_{out}^{L}&=T_{qw}^{'}T_{hw}^{'}E_{LCP}=\begin{bmatrix}2+2i & 2-2i\\ 2-2i & 2+2i\end{bmatrix}\begin{bmatrix}\cos\varphi & \sin\varphi\\ \sin\varphi & -\cos\varphi\end{bmatrix}\times\begin{bmatrix}1\\ i\end{bmatrix}=e^{i\varphi}\begin{bmatrix}0\\ 1\end{bmatrix}\\ T_{out}^{R}&=T_{qw}^{'}T_{hw}^{'}E_{RCP}=\begin{bmatrix}2+2i & 2-2i\\ 2-2i & 2+2i\end{bmatrix}\begin{bmatrix}\cos\varphi & \sin\varphi\\ \sin\varphi & -\cos\varphi\end{bmatrix}\times\begin{bmatrix}1\\ -i\end{bmatrix}=e^{-i\varphi}\begin{bmatrix}1\\ 0\end{bmatrix}.\end{aligned} \quad (6)$$

We can know that the cascaded two metasurfaces can convert the CP light into y linearly polarized (YLP) light with topological charge of +1or x linearly polarized (XLP) light with topological charge of -1 from the Eq. (6), the sign of the topological charge depends on the polarization chirality of the incident CP light.

Next, we used the CP light at 1550 nm as incident light for validating the performance of the two cascaded metasurfaces, the normalized intensity distribution and phase pattern of the transmitted light are shown in Fig. 6(b)~(e). Obviously for the LCP incident light, the YLP component of the transmitted light has become the vortex beam with topological charge of +1 while the XLP component not. Parallel results, for the RCP incident light, the XLP component has become the vortex beam with topological charge of -1 while the YLP component not. T=93.53% and $\frac{I_{YLP}}{I_{out}} = 97.57\%$ was obtained by the numerical calculation. The simulated results prove that the two cascaded metasurfaces are capable of generating vortex beam with charges of ± 1 with high efficiency, the transmitted light is linearly polarized state and the sign of charge is dependent on the handedness of incident CP light, which coincide with the Eq. (6).

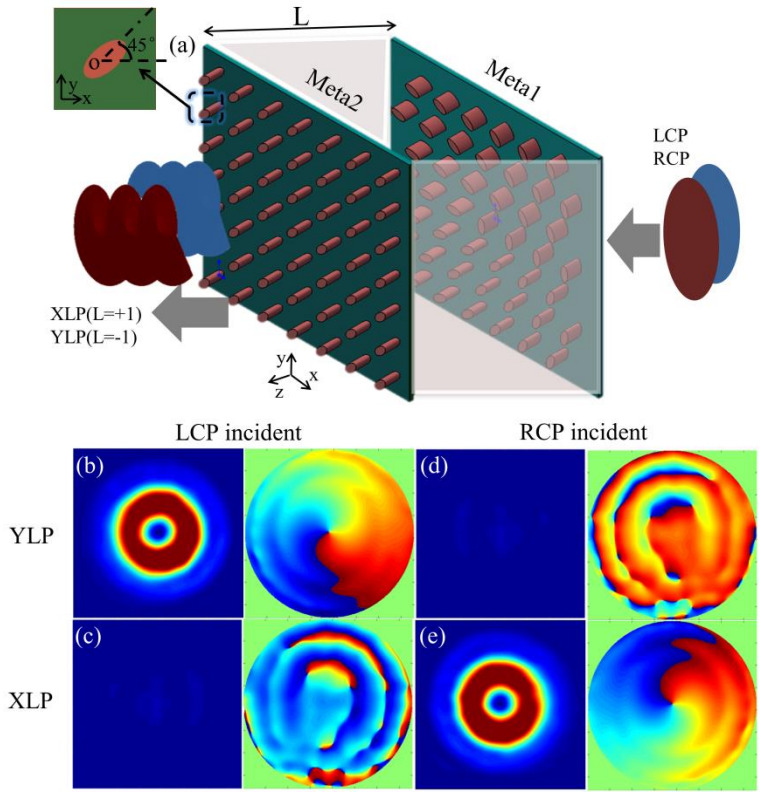

Fig. 6. (a) Schematic of the cascaded all-dielectric metasurface 1 and all-dielectric metasurface 2, Inset in (a) shows the angle of the rotation angle (α) of nanopillar equals to 45°. The intensity profile and phase pattern of (b) the YLP component and (c) the XLP component under the LCP incident light. The intensity profile and phase pattern of (d) the YLP component and (e) the XLP component under the RCP incident light (color online)

Last, we added the metasurfaces 1 after the two cascaded metasurfaces to form the three cascaded metasurfaces, the distant between the metasurfaces 1 and the metasurfaces 2 both was set to *L*, as shown in Fig. 7(a). When the CP light pass through the three metasurfaces in sequence, neglecting the constant phase, the Jones expression of the transmitted light can be expressed as:

$$\begin{aligned} T_{out}^{L} &= T_{hw}^{'}T_{qw}^{'}T_{hw}^{'}E_{LCP} = \begin{bmatrix} \cos\varphi & \sin\varphi \\ \sin\varphi & -\cos\varphi \end{bmatrix}\begin{bmatrix} 2+2i & 2-2i \\ 2-2i & 2+2i \end{bmatrix} \\ &\times \begin{bmatrix} \cos\varphi & \sin\varphi \\ \sin\varphi & -\cos\varphi \end{bmatrix}\begin{bmatrix} 1 \\ i \end{bmatrix} = e^{i\varphi}\begin{bmatrix} \sin\varphi \\ -\cos\varphi \end{bmatrix} \\ T_{out}^{R} &= T_{hw}^{'}T_{qw}^{'}T_{hw}^{'}E_{RCP} = \begin{bmatrix} \cos\varphi & \sin\varphi \\ \sin\varphi & -\cos\varphi \end{bmatrix}\begin{bmatrix} 2+2i & 2-2i \\ 2-2i & 2+2i \end{bmatrix} \\ &\times \begin{bmatrix} \cos\varphi & \sin\varphi \\ \sin\varphi & -\cos\varphi \end{bmatrix}\begin{bmatrix} 1 \\ -i \end{bmatrix} = e^{-i\varphi}\begin{bmatrix} \cos\varphi \\ \sin\varphi \end{bmatrix}. \end{aligned} \tag{7}$$

As a result, we can know that the three cascaded metasurfaces can convert the CP light into the azimuthally polarized (AP) light with topological charge of +1or the radially polarized (RP) light with topological charge of -1 from the Eq.(7), the sign of the topological charge depends on the polarization chirality of the incident CP light equally.

We still used the CP light at 1550 nm as incident light for validating the performance of the three cascaded metasurfaces, the normalized intensity distribution and phase pattern of the transmitted light are shown in Fig. 7(b)~(d). Obviously for the LCP incident light, the transmitted light has become the azimuthally polarized beam with topological charge of +1. To verify the azimuthally polarized property of the output beam, the linear polarizers in different polarization directions were mounted after the cascaded metasurfaces, as shown in Fig. 7(c)~(g). The yellow arrows denote linear

polarizer's directions (0^o, 90^o, 135^o). The transmitted light through the linear polarizers is decomposed into two parts distributed symmetrically at the center of beam. And the line between the two spots keeps vertical to the polarization direction of the linear polarizer. It also indicates the polarization order of the azimuthally polarized beam is +1. T=88.54% and $\frac{I_{AP}}{I_{out}} = 94.51\%$ was obtained by the numerical calculation. The optical field images and the results indicates that the cascaded metasurfaces are capable of generating the high-quality azimuthally polarized beam. Parallel results, for the RCP incident light, we can also know that the transmitted light has become the high-quality radially polarized beam with topological charge of -1 and polarization order of -1 according to the results and the optical field images in Fig. 7(h)~(m).

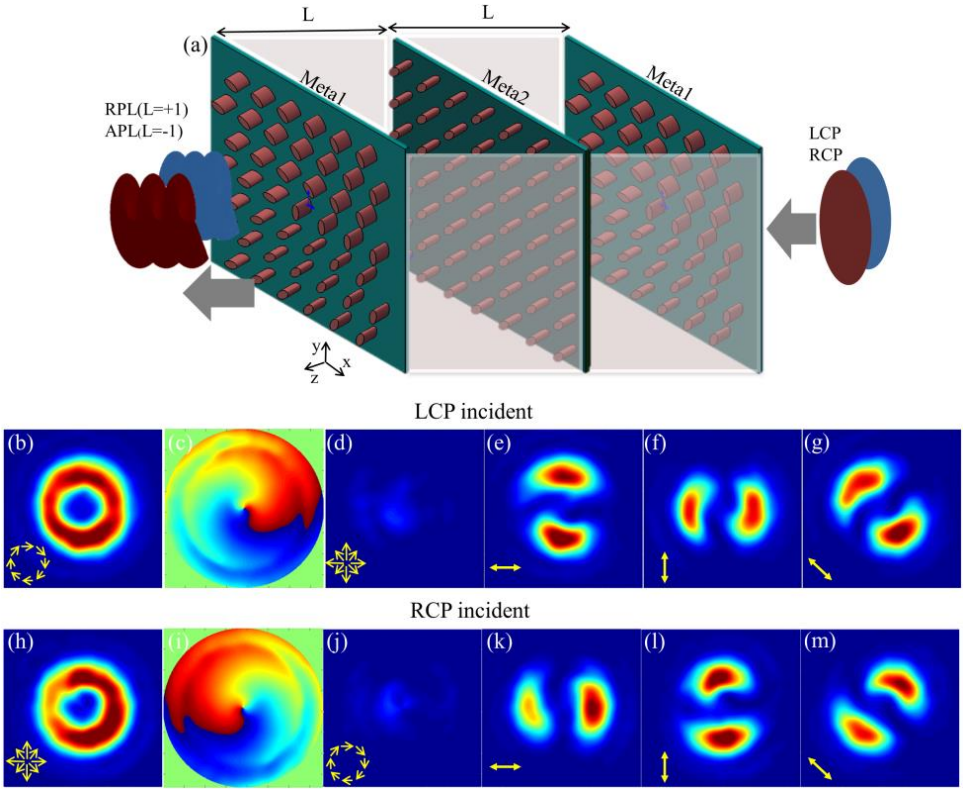

Fig. 7. (a) Schematic of the cascaded metasurface 1, metasurface 2 and metasurface 1. (b) The intensity profile and (c) phase pattern of the AP component, (d) the intensity profile of the RP component, (e)~(g) the intensity profiles of the transmitted light through the linear polarizer under the LCP incident light. (h) The intensity profile and (i) phase pattern of the RP component, (j) the intensity profile of the AP component, (k)~(m) the intensity profiles of the transmitted light through the linear polarizer under the RCP incident light. The yellow arrow denotes the direction of linear polarization (color online)

Moreover, we calculated the weight spectra of the desired topological charge, LCP light was used as incident light at 1550 nm. Vortex field distribution $E(x, y, z)$ obtained by simulation can be projected into the spiral harmonics $\exp(in\varphi)$[39, 40], where, n is topological charge, φ is azimuth angle. Vortex beam with spiral phase can be expressed as follow

$$E(\rho,\varphi,z) = \frac{1}{\sqrt{2\pi}} \sum_{n=-\infty}^{n=\infty} a_n(\rho,z)\exp(in\varphi), \tag{8}$$

where $a_n = 1/(2\pi)^{1/2} \int_0^{2\pi} E(\rho,\varphi,z)\exp(-in\varphi)d\varphi$, $E(\rho,\varphi,z)$ is the complex electric field in polar coordinates. Here, we define $C_n = \int_0^r |a_n(\rho,z)|^2 \rho d\rho$ as the weight coefficient of

the n^{th} topological charge and $P_n = 10 \times \log_{10}(C_n / \sum_{q=-\infty}^{\infty} C_q)$ as weight spectra of topological charge. We calculated the weight spectra of topological charge (±1) respectively according to Eq. (8), the results are depicted in Fig. 8. Clearly, the weight spectra of topological charges (±1) are all larger than 0.97. We defined Mode purity of vortex beam as $T \times \frac{I_{vortex}}{I_{out}} \times Weight\ spectra$, and got the value of 81.17%. The result indicates that the cascaded metasurfaces are capable of generating the high-quality vortex beam with topological charge of ± 1.

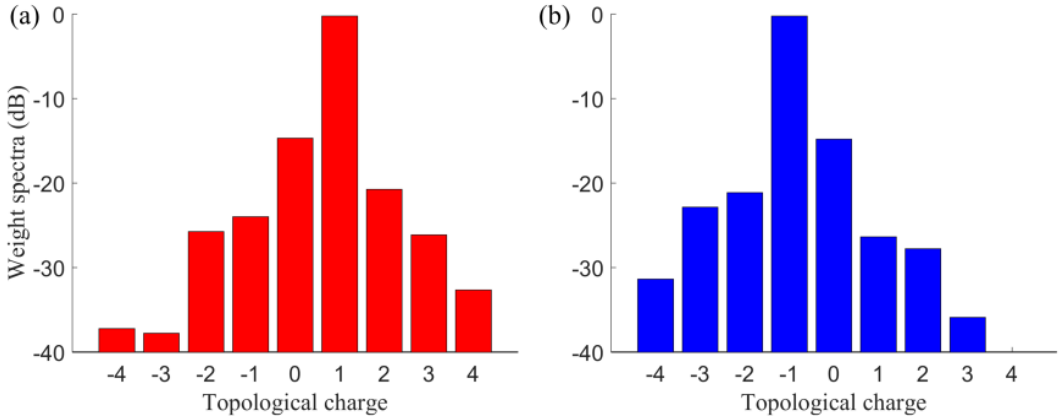

Fig. 8. Weight spectra of topological charge (a) L=+1, (b) L= -1 (color online)

Finally, the simulated results prove that the three cascaded metasurfaces are capable of generating CVV beam with high purity. The polarized state of the transmitted light is azimuthally polarized or radially polarized, the topological charge of that is ± 1 and the sign of charge is dependent on the handedness of incident CP light, which agree well with the Eq. (7). The cascaded metasurfaces has characteristics of compact, high purity, easy-fabrication which are suit for integrated photonic devices. However, it should be noted that the designed cascaded metasurfaces are capable of generating CVV beam with just fixed topological charge of ± 1 and polarization order of ± 1. The CVV beam with more topological charges and polarization orders could be achieved by inserting more metasurfaces or optimizing the design for enlarging application in integrated optics in future.

4. Conclusions

In conclusion, we propose a efficient approach to generate high-quality cylindrical vector vortex beams by cascading the three all-dielectric metasurfaces under the incidence of circularly polarized light. They operate at 1550 nm and mode purity of the CVV beam get the value of 81.71%. Simulation results agree well with theoretical derivation and validate our design. The cascaded metasurfaces have characteristics of easy-fabrication, compact, high purity without inserting any bulk optical element. Multiple topological charges and polarization orders of the transmitted beam make the designed cascaded metasurfaces suitable for the development of integrated optical system.

Acknowledgements

This work was supported by the National Natural Science Foundation of China (NSFC) (project no.61905221), the Key Scientific Research Projects in Colleges and Universities of Henan Province, China (project no. 22B140007) and the Doctoral Scientific Fund Project of Zhengzhou University of Light Industry

(project no. 2020BSJJ060).

References

[1] A. M. Yao, M. J. Padgett, Advances in Optics & Photonics **3** (2), 204 (2011).
[2] Nenad Bozinovic, Yang Yue, Yongxiong Ren, Moshe Tur, Alan E. Willner, S. Ramachandran, Science **340**, 4 (2013).
[3] L. Martin, S. Fiona, B. Stephen, P. Miles, Science **341**, 4 (2013).
[4] M. B. L Allen, R. J. C. Spreeuw, J. P. Woerdman, Physical Review A **45**(11), 8185 (1992).
[5] F. Gori, Journal of the Optical Society of America **18**(7), 11 (2001).
[6] M. Meier, V. Romano, T. Feurer, Applied Physics A **86**(3), 6 (2007).
[7] Z. Qiwen, Optics Express **12**, 6 (2004).
[8] X. Yi, X. Ling, Z. Zhang, Y. Li, X. Zhou, Y. Liu, S. Chen, H. Luo, S. Wen, Optics Express **22**(14), 15 (2014).
[9] X. Yi, P. Huang, X. Huang, Z. Xu, C. Zhang, J. Zhao, X. Liu, Y. Ai, H. Chen, Applied Physics B **123**(9), 6 (2017).
[10] C. W. Ziru Cai, Jing Jiang, Yingtao Ding, Fei Ding, Opt. Express **29**(26), 9 (2021).
[11] J. Wang, J. Du, Applied Sciences **6**, 10 (2016).
[12] Qiong He, Shulin Sun, Shiyi Xiao, Lei Zhou, Advanced Optical Materials **6**, 23 (2018).
[13] X. G. Luo, Science China (Physics,Mechanics & Astronomy) **58**(9), 19 (2015).
[14] N. Yu, P. Genevet, M. A. Kats, F. Aieta, J.-P. Tetienne, F. Capasso, Z. Gaburro, Science **334**(6054), 333-7 (2011).
[15] L. Huang, X. Chen, H. Mühlenbernd, H. Zhang, S. Chen, B. Bai, Q. Tan, G. Jin, K. W. Cheah, C. W. Qiu, Nature Communications **4**(7), 2808 (2013).
[16] Y. Liu, X. Ling, X. Yi, X. Zhou, S. Chen, Y. Ke, H. Luo, S. Wen, Optics Letters **40**(5), 4 (2015).
[17] F. Monticone, A. Alù, Chinese Physics B **23**(4), 9 (2014).
[18] L. Huang, X. Chen, H. Mühlenbernd, G. Li, B. Bai, Q. Tan, G. Jin, T. Zentgraf, S. Zhang, Nano Letters **12**(11), 6 (2012).
[19] H. X. Xu, H. Liu, X. Ling, Y. Sun, F. Yuan, IEEE Transactions on Antennas & Propagation **65**(12), 5 (2017).
[20] F. Bouchard, I. D. Leon, S. A. Schulz, J. Upham, E. Karimi, R. W. Boyd, Applied Physics Letters **105**(10), 5 (2014).
[21] F. Ed, E. Bouchard, I. D. Leon, S. A. Schulz, J. Upham, E. Karimi, R. W. Boyd, Applied Physics Letters **105**(10), 7 (2014).
[22] Z. Liu, Z. Li, L. Zhe, C. Hua, W. Liu, C. Tang, C. Gu, J. Li, H. T. Chen, S. Chen, ACS Photonics **4**(8), 9 (2017).
[23] X. Zhang, D. Kong, Y. Yuan, S. Mei, G. Wang, Optics Communications **465**, 7 (2020).
[24] Xiaodong Zhang, Fengxiao Zhai, Journal of Light Industry **36**(3), 10 (2021).
[25] A. I. Kuznetsov, A. E. Miroshnichenko, M. L. Brongersma, Y. S. Kivshar, B. Lukyanchuk, Science **354**(6314), 2472 (2016).
[26] Y. H. Fu, A. I. Kuznetsov, A. E. Miroshnichenko, Y. F. Yu, B. Lukyanchuk, Nature Communications **4**(2), 5 (2013).
[27] U. Zywietz, A. B. Evlyukhin, C. Reinhardt, B. N. Chichkov, Nature Communications **5**(s 1–4), 5 (2014).
[28] S. Sun, Z. Zhou, C. Zhang, Y. Gao, Z. Duan, S. Xiao, Q. Song, ACS Nano **11**(5), 8 (2017).
[29] Y. He, H. Ye, J. Liu, Z. Xie, D. Fan, IEEE Photonics Journal **9**(99), 9 (2017).
[30] A. Mcclung, M. Mansouree, A. Arbabi, Light: Science & Applications **9**(93), 9 (2020).
[31] P. Bootpakdeetam, H. Hemmati, R. Magnusson, Optics Letters **45**(24), 4 (2020).
[32] F. Yue, D. Wen, J. Xin, B. D. Gerardot, J. Li, X. Chen, ACS Photonics **3**(9), 8 (2016).
[33] Z. Bomzon, G. Biener, V. Kleiner, E. Hasman, Optics Letters **27**(13), 1141- (2002).
[34] S. Jahani, Z. Jacob, Nature Nanotechnology **11**(1), 4 (2016).
[35] A. A. E Arbabi, S. M. Kamali, Y. Horie, A. Faraon, Optica **4**(6), 8 (2017).
[36] X. Zhang, D. Kong, S. Liu, H. Wang, Journal of the Optical Society of America A **37**(11), 1731 (2020).
[37] S. Pancharatnam, Proceedings of the Indian Academy of Sciences - Section A **44**, 15 (1956).
[38] Z. E. Bomzon, V. Kleiner, E. Hasman, Optics Letters **26**(18), 6 (2001).
[39] L. Torner, J. Torres, S. Carrasco, Optics Express **13**(3), 8 (2005).
[40] N. Yu, P. Genevet, F. Aieta, M. A. Kats, R. Blanchard, G. Aoust, J. P. Tetienne, Z. Gaburro, F. Capasso, IEEE Journal of Selected Topics in Quantum Electronics **19**(3), 25 (2013).

*Corresponding author: zhangxiaodong@zzuli.edu.cn